MagicWand: A Single, Designed Peptide That Assembles to Stable, Ordered α-Helical Fibers[†]

Christopher Gribbon,[‡] Kevin J. Channon,[‡] Weijie Zhang,[‡] Eleanor F. Banwell,[‡] Elizabeth H. C. Bromley,[‡] Julian B. Chaudhuri,[§] Richard O. C. Oreffo,[∥] and Derek N. Woolfson*[,‡,⊥]

School of Chemistry, University of Bristol, Bristol, BS8 1TS, U.K., Department of Chemical Engineering, University of Bath, Bath, BA2 7AY, U.K., Bone and Joint Research Group, Institute of Developmental Sciences, University of Southampton, Southampton SO16 6YD, U.K., and Department of Biochemistry, University of Bristol, Bristol, BS8 1TD, U.K.

Received June 6, 2008; Revised Manuscript Received August 9, 2008

ABSTRACT: We describe a straightforward single-peptide design that self-assembles into extended and thickened nano-to-mesoscale fibers of remarkable stability and order. The basic chassis of the design is the well-understood dimeric α-helical coiled-coil motif. As such, the peptide has a heptad sequence repeat, ***abcdefg***, with isoleucine and leucine residues at the ***a*** and ***d*** sites to ensure dimerization. In addition, to direct staggered assembly of peptides and to foster fibrillogenesis—that is, as opposed to blunt-ended discrete species—the terminal quarters of the peptide are cationic and the central half anionic with lysine and glutamate, respectively, at core-flanking ***e*** and ***g*** positions. This +,−,−,+ arrangement gives the peptide its name, MagicWand (MW). As judged by circular dichroism (CD) spectra, MW assembles to α-helical structures in the sub-micromolar range and above. The thermal unfolding of MW is reversible with a melting temperature >70 °C at 100 μM peptide concentration. Negative-stain transmission electron microscopy (TEM) of MW assemblies reveals stiff, straight, fibrous rods that extended for tens of microns. Moreover, different stains highlight considerable order both perpendicular and parallel to the fiber long axis. The dimensions of these features are consistent with bundles of long, straight coiled α-helical coiled coils with their axes aligned parallel to the long axis of the fibers. The fiber thickening indicates inter-coiled-coil interactions. Mutagenesis of the outer surface of the peptide—*i.e.*, at the ***b*** and ***f*** positions—combined with stability and microscopy measurements, highlights the role of electrostatic and cation−π interactions in driving fiber formation, stability and thickening. These findings are discussed in the context of the growing number of self-assembling peptide-based fibrous systems.

The design of self-assembling biomolecular fibrous systems presents challenges in fundamental science, and potentially opens new routes to biomaterials for applications in bionanotechnology. Even restricting the scope to peptide- and protein-based systems this is a broad and active research field. For instance, though peptide fibers based on amyloid-like peptides led the way to new fibrous and gelling biomaterials (*1*−*3*), these have been joined by peptide−organic hybrids (e.g., peptide amphiphiles) (*4*), protein-based assemblies (*5*−*7*), recombinant silks (*8*), "simple" dipeptide systems (*9, 10*), peptides that mimic collagen self-assembly (*11*−*14*), and more latterly a β-peptide system (*15*). The field has been reviewed from a number of perspectives in recent years (*16*−*19*).

Of particular interest to us and a number of others is a growing class of rational peptide-fiber designs based on the α-helical coiled coil (*18*). This use of the α-helix as the building block sets the designs apart from those listed above, which predominantly center on β-structure, and it allows a wealth of protein-folding and design knowledge to be brought to the field (*20*−*22*). This understanding stems from relatively straightforward relationships between coiled-coil sequence and structures, Figure 1: most coiled-coil sequences display a heptad repeat of hydrophobic (***h***) and polar (***p***) residues, ***hpphppp***, often designated ***abcdefg***. When configured into an α-helix the hydrophobic residues at ***a*** and ***d*** are brought together to form an amphipathic structure. Two or more such helices can associate through their hydrophobic faces to form helical ropelike structures. These present perfect starting points for engineering fibrous materials; indeed, in Nature coiled coils occur in a variety of fibers including components of cytoskeletons and extracellular matrices (*23*). The structural variety in coiled coils is vast (*21*). However, rules are emerging that link certain coiled-coil sequence features to structures and thus allow confident *de novo* designs (*22*).

[†] This work was funded by the BBSRC of the U.K. *via* grants to D.N.W., J.B.C. and R.O.C.O. (companion grants E20126, E20124 and E20122, respectively) and D.N.W. (E022359).

* Corresponding author. Mailing address: School of Chemistry, University of Bristol, Bristol, BS8 1TS, U.K. Tel: 0117 95 46347. Fax: 0117 929 8611. E-mail: D.N.Woolfson@bristol.ac.uk.

[‡] School of Chemistry, University of Bristol.

[§] University of Bath.

[∥] University of Southampton.

[⊥] Department of Biochemistry, University of Bristol.

[1] Abbreviations: CD, circular dichroism; HPLC, high-performance liquid chromatography; MALDI-TOF, matrix-assisted laser desorption ionization−time of flight; MW, MagicWand; MW*x*, MagicWand variant, where *x* varies to indicate a particular variant; PBS, phosphate-buffered saline; SAF, self-assembled fiber; TEM, transmission electron microsopy; T_M, melting temperature; XRD, X-ray diffraction.

10.1021/bi801072s CCC: $40.75
Published on Web 09/04/2008

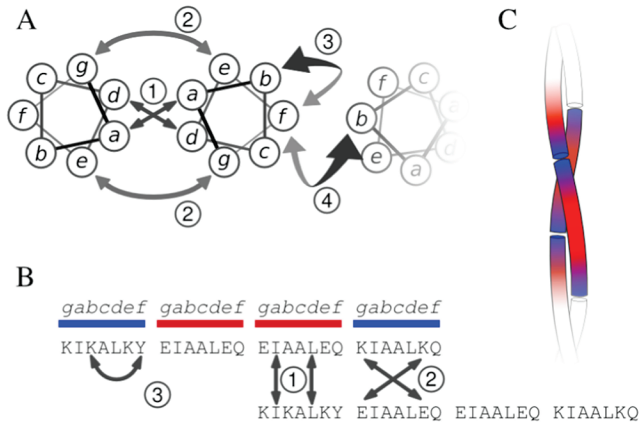

FIGURE 1: Illustrations of the design rules employed in the MW1[1] peptide. (A) Helical-wheel representations for two α-helices showing various coiled-coil interactions: 1, hydrophobic packing; 2, charge−charge interactions; and intrahelical (3) and interhelical (4) cation−π interactions. (B) Amino acid sequence of MW1 with interactions 1−3 from (A). (C) Cartoon of the coiled-coil target structure for MW1 illustrating the charge-matching principle aimed to drive sticky-ended and fiber assembly.

To our knowledge, the first report of α-helix-based peptide fibers is from Kojima and colleagues (*24*). Kajava and co-workers present a design using pentameric coiled-coil assemblies (*25*), and have supplemented it with the RGD motif for cell binding (*26*). Conticello and colleagues describe a peptide design that assembles in an offset manner (see below) to promote fiber growth along the coiled-coil helical axis (*27*). Recently, they present redesigns that switch conformation in response to pH and metal chelation (*28, 29*). Many of these coiled-coil assemblies thicken to give fibers tens of nanometers in diameter. In a bid to control such thickening, Fairman and co-workers have designed a "bi-faceted" coiled-coil peptide to promote longitudinal assembly (*30*). Another class of α-helix based fibers has been reported in which the α-helices lie perpendicular to the long axis of the fibers (*31*).

The above examples are all for what might be termed single-peptide designs. Our own work began in 2000 with the report of the first dual-peptide system (*32*). This brings the advantage that fibrillogenesis can be controlled and initiated simply by mixing the peptides, albeit at the added expense of a second designed peptide. These so-called Self-Assembled Fibers, SAFs,[1] comprise two short peptides, SAF-p1 and SAF-p2, designed *de novo* to coassemble to form an offset, or sticky ended dimer in water. The design principles are detailed in the Results section as they are pertinent to the new designs presented herein. Briefly, however, the original SAFs are 28-residue peptides with 4 canonical heptad, ***abcdefg***, repeats. The offset heterodimer is directed by a combination of jigsaw-puzzle-like hydrophobic contacts between ***a*** and ***d*** residues in the dimer interface, complementary electrostatic residues between ***g*** and ***e*** sites, Figure 1, and a buried pair of hydrogen-bonding asparagine residues at offset ***a*** sites in the two peptides. Similarly, the overhanging ends were made complementary for each other to promote fibrillogenesis (*32*). We have demonstrated and characterized the SAF designs using a combination of solution-phase spectroscopy, electron microscopy and X-ray diffraction (*32*−*34*): the fibers are straight, unbranched, solid and rigid rods with approximate dimensions of 50 nm thick and 10 μm long; they are polar structures and exhibit a considerable degree of internal order, which is observed as very well-defined reflections in X-ray fiber diffraction studies (*34*), and visible ultrastructure (by transmission electron microscopy, TEM). We have also demonstrated that SAF system can be supplemented with other, *special*, peptides to introduce branches, kinks, and cross-links to the assemblies, and to decorate them with small and large molecules (*35*−*37*). Most recently, we have chemically modified the SAFs to make extremely long synthetic polypeptides in the MDa range (*38*), and fibers of varying thickness and stiffness (*33, 39*).

The aim of the new designs presented here was to capture the structural features and engineering utility of the SAF system in a more tractable and stable single peptide system, to allow the use of these peptide fibers in cell-culture and tissue-engineering applications. To this end, we designed and characterized the MagicWand peptide. This assembles to extended and thickened fibers with structures and ultrastructure similar to the SAFs, but with much improved thermal stability. Moreover, the new systems highlighted hitherto unnoticed potential interactions within the fibers, which we were able to probe efficiently through mutagenesis because of the synthetic accessibility of MagicWand.

MATERIALS AND METHODS

Peptide Synthesis and Purification. Peptides were synthesized by standard Fmoc-based solid-phase peptide synthesis. Amino acids were obtained from Novabiochem (Merck KgaA, Darmstadt, Germany). The synthesizer used was a Protein Technologies PS3 (Tuscon, AZ). Peptides were purified by reverse-phase HPLC on a semipreparative Vydac C8 column (Grace Davison Discovery Sciences, Deerfield, IL), using a Jasco HPLC system (JASCO, Great Dunmow, Essex, U.K.). HPLC fractions were checked for the presence and purity of the required peptide by MALDI-TOF mass spectrometry and analytical HPLC. Peptide stocks were prepared from the purified fractions, and were lyophilized before being stored at −80 °C. Stocks for use in subsequent experiments were prepared in ultrapure water.

Peptide-Concentration Determination. Peptide stock concentrations were determined by UV/vis spectrometry in a Perkin-Elmer Lambda 25 UV−visible spectrophotometer, using a molar extinction coefficient, ε_{280}, of 1280 M^{-1} cm^{-1}. Peptides lacking a tyrosine were determined by measuring the absorbance of the peptide backbone and ε_{230} = 12100 M^{-1} cm^{-1}, which was back calculated from equivalent measurements of the parent, tyrosine-containing MagicWand peptide of known concentration.

Circular Dichroism Spectroscopy. Circular dichroism spectroscopy was performed in a Jasco J-810 spectropolarimeter, using the supplied software for acquisition and analysis. Measurements were taken in 0.1 cm Spectrosil quartz cuvettes. Typically, spectra were recorded for 500 μL samples, 100 μM in PBS (Sigma P4417). Machine settings were bandwidth 1 nm; in the range 260−190 nm; scanning speed 20 nm min^{-1}; averaged over two acquisitions. Melting and cooling data were acquired at a wavelength of 222 nm, with a bandwidth 2 nm, and ΔT = 60 °C h^{-1}. All experiments repeated a minimum of three times.

Transmission Electron Microscopy. Typically, peptide samples were 50 μL in volume, 100 μM peptide in PBS,

and incubated in a Techne Progene thermal cycler prior to preparation for TEM. Samples were melted at 99 °C for 300 s, then incubated at 37 °C for 48 h. For staining, 6 μL of these annealed samples were placed on carbon-coated copper grids, washed once with ultrapure water, and allowed to air-dry for ~300 s. Samples were then stained with 6 μL of either 1% uranyl acetate (Agar R1260A) or 1% ammonium dimolybdate (Agar R1156) in ultrapure water, washed in water again, and then air-dried. Grids were examined in a Phillips CM100 transmission electron microscope; scales were calibrated with a catalase crystal grid (Agar 124). Typically, images were acquired at 80 kV, at 1950× magnification or 180000× magnification, using a Kodak Megaplus 1.4i digital camera and AnalySYS iTEM software; image analysis was performed using ImageJ 1.34S software (*40*).

RESULTS

MagicWand Design Principles. The design of MagicWand-1 (MW1) used well-established sequence-to-structure relationships for coiled coils (*22*). First, the peptide had a canonical heptad repeat (***hpphppp***; ***abcdefg***) of hydrophobic (***h***) and polar (***p***) residues, Figure 1. Specifically, isoleucine (I) was placed at all ***a*** sites and leucine (L) at all ***d*** sites, which largely define the hydrophobic interface of coiled coils (*21*). This "IL" pattern strongly promotes coiled-coil dimers (*22*). Four such heptads were used, making MW1 28-residues long. In our foregoing SAF designs (*32, 33*), we guide dimeric, sticky ended coiled-coil assembly further with complementary, but offset asparagine pairs at ***a*** sites of the otherwise hydrophobic core. While conferring heterospecificity in SAFs, this generally destabilizes coiled-coil assemblies (*41*). Since we aimed to maximize the thermodynamic stability of MW1, asparagine pairs were not included at any ***a*** positions in the design of MW1. Instead, to favor a staggered alignment of helices, we used only charged interactions between the core-flanking ***e*** and ***g*** positions (*22*), Figure 1. We engineered a palindromic charge pattern along the peptide: the terminal heptads were positively charged (***g*** = ***e*** = lysine) and the central two heptads negatively charged (***g*** = ***e*** = glutamic acid), Figure 1. This +,−,−,+ pattern contrasts with the +,+,−,− arrangement of charged heptads in the original SAFs (*32, 33*). Finally, to improve solubility and ease purification, an additional lysine was included at the first ***b*** site, and a tyrosine chromophore at the first ***f***. The sequences of MW1 and its variants (see below) are given in Table 1.

MagicWand Forms Stable, α-Helical Assemblies in Solution. With future cell-culture applications of MagicWand peptides in mind, we tested the folding and assembly of 100 μM MW1 in phosphate-buffered saline (PBS, 10 mM phosphate, 137 mM NaCl, pH 7.4) at 37 °C. The circular dichroism (CD) spectrum under these conditions indicated predominantly α-helical structure, Figure 2 and Table 2. The thermal unfolding and refolding of MW1 in the range 37−95 °C was monitored using the CD signal at 222 nm ($[\theta]_{222}$) with temperature, Figure 2. Interestingly, the following behavior was reproducibly observed: the first unfolding curve showed a midpoint (T_M) of 68 ± 1 °C; the subsequent refolding curve showed marked hysteresis from the melt with a lower T_M (60 ± 1 °C); unfolding was fully reversible; moreover, the refolded material had an increased ellipticity, and subsequent melting curves consistently returned a stabilized T_M of 73 ± 1 °C. The thermal unfolding and refolding behavior of MW1 was also concentration-dependent, consistent with oligomerization of peptides as designed. However, it was not possible to determine a lower-limit in peptide folding as this was below the μM concentration limits required for reliable CD spectroscopy (see below).

MagicWand Forms Ordered Fibers. Negative-stain transmission electron microscopy (TEM) confirmed that MW1 formed fibers as designed, Figure 3. Fibers were observed over the range pH 6−9.0. Moreover, at neutral pH, fibers were observed by TEM down to 250 pM peptide. In all cases, the fibers had similar morphologies to the previous, dual-

Table 1: Summary of Designed Peptide Sequences[a]

Peptide	Sequence *gabcdefgabcdefgabcdefgabcdef*
MW1	**K**I**K**A**L**K**Y**E**I**A**A**L**E**Q**E**I**A**A**L**E**Q**K**I**A**A**L**K**Q**
MW1-K3A	**K**I**A**A**L**K**Y**E**I**A**A**L**E**Q**E**I**A**A**L**E**Q**K**I**A**A**L**K**Q**
MW1-Y7Q	**K**I**K**A**L**K**Q**E**I**A**A**L**E**Q**E**I**A**A**L**E**Q**K**I**A**A**L**K**Q**
MW1-K3E	**K**I**E**A**L**K**Y**E**I**A**A**L**E**Q**E**I**A**A**L**E**Q**K**I**A**A**L**K**Q**
MW1-K3nL	**K**I**n**A**L**K**Y**E**I**A**A**L**E**Q**E**I**A**A**L**E**Q**K**I**A**A**L**K**Q**
MW1-Y7→21	**K**I**K**A**L**K**Q**E**I**A**A**L**E**Q**E**I**A**A**L**E**Y**K**I**A**A**L**K**Q**
MW1-K3→17	**K**I**A**A**L**K**Y**E**I**A**A**L**E**Q**E**I**K**A**L**E**Q**K**I**A**A**L**K**Q**

[a] Key: Sequences start at ***g*** and end at ***f*** because ***g***−***e*** interactions are between successive heptads; green **n** represents nor-leucine.

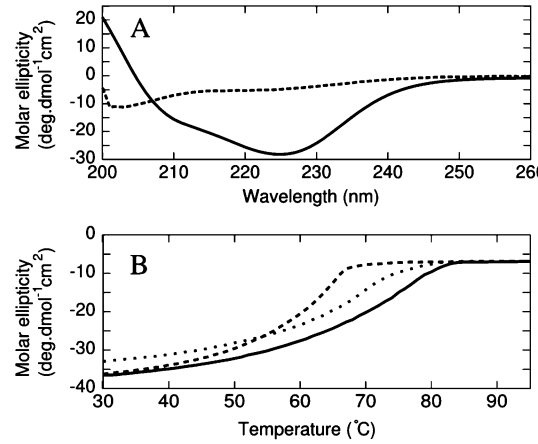

FIGURE 2: Data from circular dichroism (CD) spectroscopy. (A) CD spectra of MW1 at 37 °C (solid line) and 95 °C (dashed) showing helical structure that is lost upon heating. (B) A series of repeated heating/cooling steps of MW1, showing the hysteresis and annealing that occur between the melt (solid) and cool (dashed) phases. The initial melt of the sample is also shown (dotted).

Table 2: Summary of the CD Spectroscopy and TEM Data for the MW−Peptide Assemblies[a]

peptide	θ_{222} (deg·dmol^{-1}cm^2)	T_M 2nd melt (°C)	fiber width (nm)
MW1	−31.2 ± 0.1 (13)	73 ± 1 (6)	90 ± 30 (48)
MW1-K3A	−20 ± 1.1 (10)	73 ± 1 (3)	fibers not obsd
MW1-K3E	−19.9 ± 0.1 (6)	55 ± 1 (3)	fibers not obsd
MW1-K3nL	−28.5 ± 0.5 (4)	64 ± 2 (4)	fibers not obsd
MW1-Y7Q	−27.9 ± 0.9 (9)	66 ± 4 (3)	13 ± 3 (50)
MW1-Y7→21	−28.5 ± 1.1 (20)	66 ± 2 (6)	150 ± 1; 30 (208)
MW1-K3→17	−17.7 ± 0.1 (15)	65 ± 2 (4)	fibers not obsd

[a] The uncertainties are given as standard errors from analyses of *n* observations (values of *n* are given in parentheses).

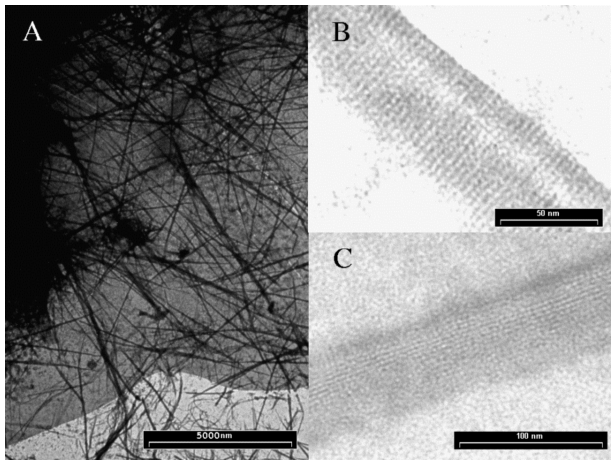

FIGURE 3: Transmission electron microscopy (TEM) images of MW1 fibers. (A) Low magnification view showing a field of typical MW1 fibers. (B) Magnified image with ammonium molybdate staining showing a striation pattern perpendicular to the long axis of the fiber. (C) Magnified view with uranyl acetate staining showing lateral stripes.

peptide, SAF designs, confirming that sticky ended assembly is achievable entirely by interactions mediated through the ***e*** and ***g*** positions, and without buried polar residues. Specifically, MW1 fibers were long (on the order of tens of microns), straight, unbranched and considerably thicker (90 ± 30 nm; $n = 48$) than expected for a stand-alone coiled coil (~2 nm). Moreover, upon staining with ammonium molybdate, the fibers displayed a regular, repeating striation pattern perpendicular to the long fiber axis, Figure 3B. Fourier transformation of pixel intensity data from TEM micrographs revealed a striation periodicity of 4.34 ± 0.24 nm ($n = 102$), which correlates well with the peptide folded as an α-helical coiled coil as designed; 28 residues with a 0.148 nm rise per residue = 4.14 nm. As noted for the SAF designs (*39*), we interpret this as positive staining, indicating peptide monomers aligned parallel to the long axis of the fiber. Interestingly however, when stained with uranyl acetate, MW1 fibers did not show striations, but were striped along their long axis, Figure 3C. The periodicity of these stripes was ~ 3.5 ± 0.04 nm ($n = 24$). We have not observed this type of patterning before in the related SAF systems. We posit that this is standard negative staining that reflects ordered bundling of long, straight coiled coils, possibly into hexagonal arrays, as observed for the SAFs by X-ray fiber diffraction (*34*).

Mutagenesis of MagicWand: Investigating the Roles of Surface Lysine and Tyrosine Residues. It is interesting that MW1 forms thickened, ordered fibers like the SAF systems, as it lacks certain design features of the SAFs. In particular, the ordering within SAF structures is likely related to amino acids—and particularly combinations of charged residues—on the outer surfaces of the coiled coils, i.e. at ***b***, ***c*** and ***f*** (*33, 34, 39*). The corresponding residues of MW1 are largely alanines and uncharged glutamines, that is, with the exception of a lysine at position 3 (K3, a ***b*** site) and a tyrosine at 7 (Y7, an ***f*** site), which were included for practical reasons noted above. Serendipitously, these residues were placed at positions i and $i + 4$ in the peptide sequence, which opens possibilities for both intrahelical and inter-coiled-coil interactions. As detailed in the Discussion, there are a number of forms that these potential interactions could take, for instance intrahelical cation−π and/or interhelical π−π or cation−π interactions (*42*). To test the possibilities, we made a series of point and paired mutations to the MW1 sequence, Table 1, and characterized these by CD spectroscopy and negative-stain TEM (Table 2).

Lysine-3 can interact with the phenyl ring of tyrosine-7 either via its charged ε-amino group or through hydrophobic interactions with the alkyl portion of the side-chain. To probe these possibilities, three mutants were made at lysine-3: MW1-K3E, in which glutamic acid was used to switch the side-chain, and overall peptide charge from cationic to anionic; MW1-K3A, where the lysine was replaced by alanine, which is used at all other ***b*** sites of the design; and MW1-K3nL, where nor-leucine was used to remove just the ε-amino group of the lysine leaving its four-carbon hydrophobic component. Like the parent, all three mutants displayed concentration-dependent α-helical CD spectra and melting behaviors; although the intensities of $[\theta]_{222}$ signals for MW1-K3A and MW1-K3E were significantly reduced, as were the T_M values for MW1-K3E and MW1-K3nL, Table 2. Despite this stable α-helical folding, as judged by negative-stain TEM, none of the mutants formed thickened and ordered fibers like the parent. Assembly was attempted over a range of temperatures (4−37 °C), but none yielded fibers.

Two other mutants centered on tyrosoine-7. First in MW1-Y7Q, it was replaced by glutamine, the residue at all other ***f*** positions of the sequence. Like the aforementioned mutants this variant had similar solution-phase α-helical and melting properties to MW1, Table 2. In addition however, MW1-Y7Q formed tangled networks, though these contained much thinner fibers than those formed by the parent, Table 1. Also, despite closely similar sample preparation, these fibers did not display the striated pattern characteristic of the thicker fibers formed by MW1. Second, to test the importance of any i, $i + 4$ interaction between lysine and tyrosine, we engineered the double mutant Y7Q plus Q21Y (named MW1-Y7→21), which, in effect, moved the tyrosine residue from the first to the third heptad repeat of the design. This is an anagram mutation because the amino acid composition is unchanged. In this case, the CD characteristics were very similar to MW1 and the point mutants, Table 2. Unlike the other mutants, MW1-Y7→21 did form thickened fibers, striped and striated similar to MW1, Figure 4.

This mutagenesis analysis shows a role for both K3 and Y7 in the formation of thickened and ordered fibers in the MW system. The MW1-K3nL mutant in particular highlights that cation−π interactions probably contribute to fiber thickening. Moreover, the formation of ordered fibers by the MW1-Y7→21 anagram mutant indicates that this interaction does not require the cationic and aromatic components to be spaced compatible with an intrahelical interaction, or indeed even within the same heptad. Therefore, the Lys−Tyr interaction must be an inter-coiled-coil interaction, though for MW1 itself it is potentially both intrahelical and inter-coiled coil.

N.b., regarding the folding of the other mutant sequences to stable α-helical oligomers that do not lead to perceptible fibers, this is becoming a general phenomenon, which we and others are beginning to explore (*39*).

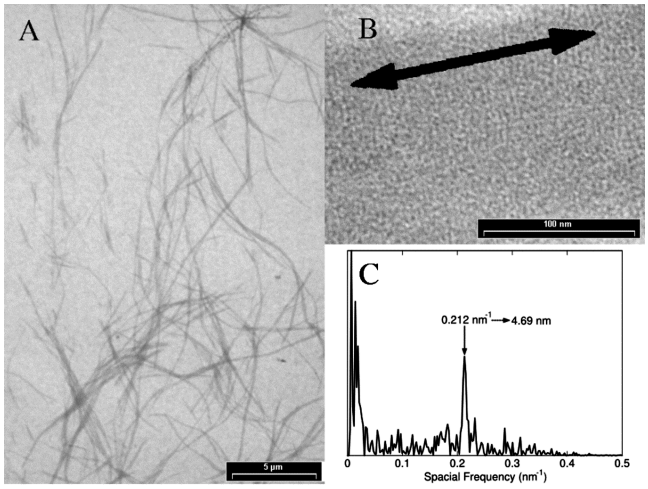

FIGURE 4: TEM images of MW1-Y7→21 fibers. (A) At low magnification showing a field of typical MW1-Y7→21 fibers. (B) A magnified view of a fiber stained with ammonium molybdate showing striations. The arrow indicates the direction of the long axis of the fiber. (C) Fourier transform analysis of the image in B which shows a clear peak corresponding to one peptide length.

DISCUSSION

In summary, the MagicWand (MW) design relies solely on pairing hydrophobic residues in the core, and charged residues flanking the core to specify an offset parallel coiled-coil dimer, the aim being that the dimers form building blocks for peptide fibrillogenesis. Consistent with this, the parent peptide, MW1, forms extended fibers tens of microns long and tens of nanometers thick. The fibers are straight and do not branch. They display surface nanoscale features consistent with the assembly and association of α-helical coiled-coils parallel to the long axis of the fibers as designed. In these respects, MW1 captures many of the features from the foregoing SAF systems (*32, 33, 39*), but in a more-straightforward, single-peptide design.

In addition—and because we replaced the buried asparagine residues used to direct sticky ended heterodimers in the SAF systems (*32*) with isoleucine—MW1 forms stable fibers at sub-micromolar peptide concentrations and above, and with a T_M of 73 °C for 100 μM peptide preparations. These compare with critical concentrations for fiber formation (i.e., the lowest concentration at which fibers were observed) of ~60 and ~40 μM, and T_M values of 22 and 49 °C (measured at 100 μM peptide) for the first- and second-generation SAFs, respectively, which are 28-residue peptides like the MW designs (*32, 33*). The stability of MW1 is also improved over a 35-residue third-generation SAF design, which has a critical concentration of 4 μM and a T_M of 64 °C (at 100 μM peptide) (*33*). Furthermore, the thermal unfolding process in MW1 is fully reversible, which allows the system to be annealed: melting curves for freshly prepared MW1 samples have T_Ms of ~68 °C; cooling leads to increased apparent α-helicities; and subsequent remelting renders T_Ms of ~73 °C. This behavior is likely linked to the single-peptide system and its strong drive to form α-helical assemblies: once prepared MW1 forms helical structures very rapidly; we propose that at this stage, though the prominent forms are α-helical fibers, a mixture of such structures is formed; the heating−cooling−heating cycle allows any misassembled peptides, or those that are assembled as suboptimal fibers, to become incorporated into well-defined α-helical, fibrous assemblies. Thus, in comparison to the dual-peptide SAF system, one element of control over the assembly has been lost, but a considerable gain in stability is achieved together with opportunities to anneal the system.

The ease of preparation of the MW peptides and fibers presents a number of possibilities for the system, for example: to tune fiber stability; to probe sequence-to-structure relationships; and to develop potential applications for α-helical fibers. With these in mind, we have designed and characterized a series of MW1 mutants to explore the features that lead to fiber assembly, stability and thickening. We focused on two residues on the outer surface of the designed leucine-zipper dimer—i.e., those outside the core ***a***, ***d***, ***e*** and ***g*** sites of the heptad repeat—that are different from the other surface-exposed residues—namely lysine-3 and tyrosine-7, which are at ***b*** and ***f*** positions (see Figure 1A). Potentially, these residues could participate in salt-bridge, cation−π, $\pi-\pi$ or hydrophobic interactions. Another possibility is the involvement of ***f*** position glutamine residues in hydrogen-bonding networks between coiled-coil helices—interactions of this type are observed in the complex, multihelix assembly of the SARS coronavirus spike glycoprotein for example (*43*)—but these interactions were not explored directly here through mutations due to the large number of possible variants.

$\pi-\pi$, or π-stacking interactions have long been recognized as important contributors to the structure and stability of proteins and peptides (*42, 44*). For helical peptides, Aravinda et al. show that both intra- and interhelical π-stacking between phenylalanine residues along one face of a helix promote helix associations (*45*). However, for the MW system under the conditions we investigated, none of the substitutions of lysine-3 by alanine, glutamate and norleucine—which all retain the tyrosine—give supramolecular fibers. This suggests that straight hydrophobic, or $\pi-\pi$ interactions alone do not play a major role in the formation of such structures. These data also discount hydrogen bonding between glutamines at ***f*** sites playing an important role in fiber assembly, as, again, all the variants retain three such residues. Clearly, however, the mutations at lysine-3 strongly implicate a role for this positively charged residue. Moreover, the MW variants that form thickened and ordered (striated) fibers reproducibly—namely, MW1 and MW1-Y7→21—are those with both lysine and tyrosine. This suggests strongly that cation−π interactions do contribute to fiber stability and thickening and internal structure.

Similarly to $\pi-\pi$ interactions, cation−π interactions have long been considered important to protein structure, stability and function (*42, 44, 46−48*). They have been subject to detailed experimental and theoretical analyses, though their precise nature and worth remains controversial (*42, 49−52*). Specifically, potential intra- (i, $i + 3$ and i, $i + 4$) and inter-α-helical (notably between ***g*** and ***e*** sites of coiled coils) cation−π interactions have been probed (*53−55*). Though the details vary, the consensus is that the interactions are favorable even if the underlying mechanism(s) is not agreed. In this context, lysine-3 and tyrosine-7 have an i, $i + 4$ relationship in MW1, which, as illustrated by arrow 3 in Figure 1A, presents the possibility of straightforward intra-helical interactions that could stabilize the α-helical folding and thence fiber formation without necessarily cementing

fibril−fibril interactions and fiber thickening. To test this directly, we made the anagram variant MW1-Y7→21, in which the tyrosine was simply moved further away in sequence from lysine-3. This forms thickened and ordered fibers, indicating that if cation−π interactions are involved in MagicWand assembly, they act at the inter-coiled-coil level; indeed, the fibers are thicker than those formed by the parent peptide, which suggests that inter-coiled-coil cation−π interactions, as illustrated by arrow 4 in Figure 1A, may be stronger without potentially competing intrahelical interactions. Developing this theme further, two more-recent studies are relevant: Anderson et al. show that a lysine−phenylalanine interaction can occur in a peptide from the rhodopsin system, but that it is readily masked if the C-terminal carboxylic acid of the latter is free (*56*); and Berry and co-workers demonstrate that cation−π interactions are reduced upon solvent exposure (*57*). These relate to the MW system in that another anagram mutant in which the lysine-3 was moved by two heptads, MW1-K3→17, Tables 1 and 2, does not form fibers, which we suspect is due to sequestering the relocated lysine by surrounding glutamic acids at positions 13 and 20, Table 1; and that any cation−π interactions may well be better formed in the thickened, well-ordered and cooperative arrangement of the interior of the assembled fibers (*34*).

CONCLUSION

We have successfully designed a relatively straightforward, single-peptide system, MagicWand, that assembles into nano-to-mesoscale protein fibers. These are thermally stable and exhibit considerable order comparable to our earlier, more-sophisticated two-peptide designs (*32*−*34*). The relative simplicity of the system has allowed a number of mutants to be made to assess sequence-to-structure relationships. For example, we have identified potential inter-coiled-coil cation−π interactions that are important in establishing the matured, thickened fibers. Defining such interactions could help further refine three-dimensional structural models for coiled-coil fibers of the SAF and MW type, which is otherwise a daunting task (*34*). In addition, because of its ease of synthesis, solubility, faithful assembly and stability, MagicWand provides a good chassis for the development of future functional biomaterials.

REFERENCES

1. Zhang, S. G., Holmes, T., Lockshin, C., and Rich, A. (1993) Spontaneous Assembly of a Self-Complementary Oligopeptide to Form a Stable Macroscopic Membrane. *Proc. Natl. Acad. Sci. U.S.A. 90*, 3334–3338.
2. Aggeli, A., Bell, M., Boden, N., Keen, J. N., Knowles, P. F., McLeish, T. C. B., Pitkeathly, M., and Radford, S. E. (1997) Responsive gels formed by the spontaneous self-assembly of peptides into polymeric beta-sheet tapes. *Nature 386*, 259–262.
3. Schneider, J. P., Pochan, D. J., Ozbas, B., Rajagopal, K., Pakstis, L., and Kretsinger, J. (2002) Responsive hydrogels from the intramolecular folding and self-assembly of a designed peptide. *J. Am. Chem. Soc. 124*, 15030–15037.
4. Hartgerink, J. D., Beniash, E., and Stupp, S. I. (2001) Self-assembly and mineralization of peptide-amphiphile nanofibers. *Science 294*, 1684–1688.
5. Ogihara, N. L., Ghirlanda, G., Bryson, J. W., Gingery, M., DeGrado, W. F., and Eisenberg, D. (2001) Design of three-dimensional domain-swapped dimers and fibrous oligomers. *Proc. Natl. Acad. Sci. U.S.A. 98*, 1404–1409.
6. Padilla, J. E., Colovos, C., and Yeates, T. O. (2001) Nanohedra: using symmetry to design self assembling protein cages, layers, crystals, and filaments. *Proc. Natl. Acad. Sci. U.S.A. 98*, 2217–2221.
7. Scheibel, T., Parthasarathy, R., Sawicki, G., Lin, X. M., Jaeger, H., and Lindquist, S. L. (2003) Conducting nanowires built by controlled self-assembly of amyloid fibers and selective metal deposition. *Proc. Natl. Acad. Sci. U.S.A. 100*, 4527–4532.
8. Huemmerich, D., Helsen, C. W., Quedzuweit, S., Oschmann, J., Rudolph, R., and Scheibel, T. (2004) Primary structure elements of spider dragline silks and their contribution to protein solubility. *Biochemistry 43*, 13604–13612.
9. Reches, M., and Gazit, E. (2003) Casting metal nanowires within discrete self-assembled peptide nanotubes. *Science 300*, 625–627.
10. Jayawarna, V., Ali, M., Jowitt, T. A., Miller, A. E., Saiani, A., Gough, J. E., and Ulijn, R. V. (2006) Nanostructured hydrogels for three-dimensional cell culture through self-assembly of fluorenylmethoxycarbonyl-dipeptides. *Adv. Mater. 18*, 611–614.
11. Paramonov, S. E., Gauba, V., and Hartgerink, J. D. (2005) Synthesis of collagen-like peptide polymers by native chemical ligation. *Macromolecules 38*, 7555–7561.
12. Kotch, F. W., and Raines, R. T. (2006) Self-assembly of synthetic collagen triple helices. *Proc. Natl. Acad. Sci. U.S.A. 103*, 3028–3033.
13. Gauba, V., and Hartgerink, J. D. (2007) Self-assembled heterotrimeric collagen triple helices directed through electrostatic interactions. *J. Am. Chem. Soc. 129*, 2683–2690.
14. Rele, S., Song, Y. H., Apkarian, R. P., Qu, Z., Conticello, V. P., and Chaikof, E. L. (2007) D-periodic collagen-mimetic microfibers. *J. Am. Chem. Soc. 129*, 14780–14787.
15. Pomerantz, W. C., Yuwono, V. M., Pizzey, C. L., Hartgerink, J. D., Abbott, N. L., and Gellman, S. H. (2008) Nanofibers and lyotropic liquid crystals from a class of self-assembling beta-peptides. *Angew. Chem., Int. Ed. 47*, 1241–1244.
16. Rajagopal, K., and Schneider, J. P. (2004) Self-assembling peptides and proteins for nanotechnological applications. *Curr. Opin. Struct. Biol. 14*, 480–486.
17. Scheibel, T. (2005) Protein fibers as performance proteins: new technologies and applications. *Curr. Opin. Biotechnol. 16*, 427–433.
18. Woolfson, D. N., and Ryadnov, M. G. (2006) Peptide-based fibrous biomaterials: some things old, new and borrowed. *Curr. Opin. Chem. Biol. 10*, 559–567.
19. Ulijn, R. V., and Smith, A. M. (2008) Designing peptide based nanomaterials. *Chem. Soc. Rev. 37*, 664–75.
20. Doig, A. J., Errington, N., and Iqbalsyah, T. M. (2005) Stability and Design of alpha-Helices, in *Protein Folding Handbook* (Kiefhaber, T., and Buchner, J., Eds.) pp 247−299, Wiley-VCH, Weinheim, Germany.
21. Lupas, A. N., and Gruber, M. (2005) The structure of α-helical coiled-coils. *Adv. Protein Chem. 70*, 37–78.
22. Woolfson, D. N. (2005) The Design of Coiled-Coil Structures and Assemblies. *Adv. Protein Chem. 70*, 79–112.
23. Pollard, T. D., and Earnshaw, W. C. (2002) *Cell Biology*, Saunders, London.
24. Kojima, S., Kuriki, Y., Yoshida, T., Yazaki, K., and Miura, K. (1997) Fibril formation by an amphipathic α helix-forming polypeptide produced by gene engineering. *Proc. Jpn. Acad. Ser. B-Phys. Biol. Sci. 73*, 7–11.
25. Potekhin, S. A., Melnik, T. N., Popov, V., Lanina, N. F., Vazina, A. A., Rigler, P., Verdini, A. S., Corradin, G., and Kajava, A. V. (2001) De novo design of fibrils made of short α-helical coiled coil peptides. *Chem. Biol. 8*, 1025–1032.
26. Villard, V., Kalyuzhniy, O., Riccio, O., Potekhin, S., Melnik, T. N., Kajava, A. V., Ruegg, C., and Corradin, G. (2006) Synthetic RGD-containing α-helical coiled coil peptides promote integrin-dependent cell adhesion. *J. Pept. Sci. 12*, 206–212.
27. Zimenkov, Y., Conticello, V. P., Guo, L., and Thiyagarajan, P. (2004) Rational design of a nanoscale helical scaffold derived from self-assembly of a dimeric coiled coil motif. *Tetrahedron 60*, 7237–7246.
28. Zimenkov, Y., Dublin, S. N., Ni, R., Tu, R. S., Breedveld, V., Apkarian, R. P., and Conticello, V. P. (2006) Rational design of a reversible pH-responsive switch for peptide self-assembly. *J. Am. Chem. Soc. 128*, 6770–6771.
29. Dublin, S. N., and Conticello, V. P. (2008) Design of a selective metal ion switch for self-assembly of peptide-based fibrils. *J. Am. Chem. Soc. 130*, 49–51.

30. Wagner, D. E., Phillips, C. L., Ali, W. M., Nybakken, G. E., Crawford, E. D., Schwab, A. D., Smith, W. F., and Fairman, R. (2005) Toward the development of peptide nanofilaments and nanoropes as smart materials. *Proc. Natl. Acad. Sci. U.S.A. 102*, 12656–12661.
31. Lazar, K. L., Miller-Auer, H., Getz, G. S., Orgel, J., and Meredith, S. C. (2005) Helix-turn-helix peptides that form α-helical fibrils: Turn sequences drive fibril structure. *Biochemistry 44*, 12681–12689.
32. Pandya, M. J., Spooner, G. M., Sunde, M., Thorpe, J. R., Rodger, A., and Woolfson, D. N. (2000) Sticky-End Assembly of a Designed Peptide Fiber Provides Insight into Protein Fibrillogenesis. *Biochemistry 39*, 8728–8734.
33. Smith, A. M., Banwell, E. F., Edwards, W. R., Pandya, M. J., and Woolfson, D. N. (2006) Engineering Increased Stability into Self-Assembled Protein Fibers. *Adv. Funct. Mater. 16*, 1022–1030.
34. Papapostolou, D., Smith, A. M., Atkins, E. D. T., Oliver, S. J., Ryadnov, M. G., Serpell, L. C., and Woolfson, D. N. (2007) Engineering nanoscale order into a designed protein fiber. *Proc. Natl. Acad. Sci. U.S.A. 104*, 10853–10858.
35. Ryadnov, M. G., and Woolfson, D. N. (2003) Engineering the morphology of a selfassembling protein fibre. *Nat. Mater. 2*, 329–332.
36. Ryadnov, M. G., and Woolfson, D. N. (2004) Fiber recruiting peptides: Noncovalent decoration of an engineered protein scaffold. *J. Am. Chem. Soc. 126*, 7454–7455.
37. Ryadnov, M. G., and Woolfson, D. N. (2005) MaP peptides: Programming the self-assembly of peptide-based mesoscopic matrices. *J. Am. Chem. Soc. 127*, 12407–12415.
38. Ryadnov, M. G., and Woolfson, D. N. (2007) Self-assembled templates for polypeptide synthesis. *J. Am. Chem. Soc. 129*, 14074–14081.
39. Papapostolou, D., Bromley, E. H. C., Bano, C., and Woolfson, D. N. (2008) Electrostatic control of thickness and stiffness in a designed protein fiber. *J. Am. Chem. Soc. 130*, 5124–5130.
40. Abramoff, M. D., Magelhaes, P. J., and Ram, S. J. (2004) Image Processing with ImageJ. *Biophotonics Int. 11*, 36–42.
41. Gonzalez, L., Woolfson, D. N., and Alber, T. (1996) Buried polar residues and structural specificity in the GCN4 leucine zipper. *Nat. Struct. Biol. 3*, 1011–1018.
42. Waters, M. L. (2004) Aromatic interactions in peptides: Impact on structure and function. *Biopolymers 76*, 435–445.
43. Duquerroy, S., Vigouroux, A., Rottier, P. J. M., Rey, F. A., and Jan Bosch, B. (2005) Central ions and lateral asparagine/glutamine zippers stabilize the post-fusion hairpin conformation of the SARS coronavirus spike glycoprotein. *Virology 335*, 276–285.
44. Burley, S. K., and Petsko, G. A. (1985) Aromatic-Aromatic Interaction - A Mechanism of Protein-Structure Stabilization. *Science 229*, 23–28.
45. Aravinda, S., Shamala, N., Das, C., Sriranjini, A., Karle, I. L., and Balaram, P. (2003) Aromatic-Aromatic Interactions in Crystal Structures of Helical Peptide Scaffolds Containing Projecting Phenylalanine Residues. *J. Am. Chem. Soc. 125*, 5308–5315.
46. Scrutton, N. S., and Raine, A. R. C. (1996) Cation-pi bonding and amino-aromatic interactions in the biomolecular recognition of substituted ammonium ligands. *Biochem. J. 319*, 1–8.
47. Ma, J. C., and Dougherty, D. A. (1997) The cation-pi interaction. *Chem. Rev. 97*, 1303–1324.
48. Shi, Z. S., Olson, C. A., Bell, A. J., and Kallenbach, N. R. (2001) Stabilization of α helix structure by polar side-chain interactions: Complex salt bridges, cation-pi interactions, and C-H···O H-bonds. *Biopolymers 60*, 366–380.
49. Mitchell, J. B. O., Nandi, C. L., McDonald, I. K., Thornton, J. M., and Price, S. L. (1994) Amino/Aromatic Interactions in Proteins: Is the Evidence Stacked Against Hydrogen Bonding? *J. Mol. Biol. 239*, 315–331.
50. Mecozzi, S., West, J. A. P., and Dougherty, D. A. (1996) Cation-pi interactions in aromatics of biological and medicinal interest: Electrostatic potential surfaces as a useful qualitative guide. *Proc. Natl. Acad. Sci. U.S.A. 93*, 10566–10571.
51. Biot, C., Buisine, E., and Rooman, M. (2003) Free-Energy Calculations of Protein-Ligand Cation-pi and Amino-pi Interactions: From Vacuum to Proteinlike Environments. *J. Am. Chem. Soc. 125*, 13988–13994.
52. Lummis, S. C., R., L., Beene, D., Harrison, N. J., Lester, H. A., and Dougherty, D. A. (2005) A Cation-pi Binding Interaction with a Tyrosine in the Binding Site of the GABAC Receptor. *Chem. Biol. 12*, 993–997.
53. Andrew, C. D., Bhattacharjee, S., Kokkoni, N., Hirst, J. D., Jones, G. R., and Doig, A. J. (2002) Stabilizing interactions between aromatic and basic side chains in α-helical peptides and proteins. Tyrosine effects on helix circular dichroism. *J. Am. Chem. Soc. 124*, 12706–12714.
54. Tsou, L. K., Tatko, C. D., and Waters, M. L. (2002) Simple cation-pi interaction between a phenyl ring and a protonated amine stabilizes an α helix in water. *J. Am. Chem. Soc. 124*, 14917–14921.
55. Slutsky, M. M., and Marsh, E. N. G. (2004) Cation-pi interactions studied in a model coiled-coil peptide. *Protein Sci. 13*, 2244–2251.
56. Anderson, M. A., Ogbay, B., Arimoto, R., Sha, W., Kisselev, O. G., Cistola, D. P., and Marshall, G. R. (2006) Relative strength of cation-pi vs salt-bridge interactions: The G(t)alpha(340−350) peptide/rhodopsin system. *J. Am. Chem. Soc. 128*, 7531–7541.
57. Berry, B. W., Elvekrog, M. M., and Tommos, C. (2007) Environmental modulation of protein cation-pi interactions. *J. Am. Chem. Soc. 129*, 5308–5309.

BI801072S